



# Experimental Study on the Liquefaction Characteristics of Basalt Fiber-Reinforced Saturated Sand

Yu Ding<sup>1,2</sup> · Yu Jia<sup>2</sup> · Xuan Wang<sup>2</sup> · Jiasheng Zhang<sup>2</sup> · Xiaobin Chen<sup>2</sup>

Received: 20 March 2022 / Accepted: 28 October 2022 / Published online: 27 November 2022  
© The Author(s), under exclusive licence to Indian Geotechnical Society 2022

**Abstract** To study the liquefaction characteristics of fiber-reinforced saturated sand, a series of cyclic triaxial tests were carried out and analyzed the influences of basalt fiber content (FC = 0, 0.2%, 0.4%), cyclic stress ratio (CSR = 0.30, 0.35, 0.40), loading frequency ( $f = 1, 3, 5$  Hz) on the excess pore water pressure (EPWP) characteristics, and the liquefaction resistance of saturated sand and basalt fiber-reinforced saturated sand. The dynamic strength curves of saturated sand and basalt fiber-reinforced saturated sand were discussed. The research results show that the addition of basalt fiber can effectively inhibit the generation and accumulation of excess pore water pressure (EPWP) and improve the liquefaction resistance of saturated sand. As the basalt fiber content increases, the liquefaction resistance of fiber-reinforced saturated sand increases, and the optimal basalt fiber content is about 0.4%. The greater the cyclic stress ratio (CSR) and loading frequency, the more likely the saturated sand is to undergo liquefaction failure. The excess pore water pressure ratio (EPWPR) of saturated

sand and basalt fiber-reinforced saturated sand correlated with the hyperbolic model. The dynamic strength curves of saturated sand and basalt fiber-reinforced saturated sand conformed to the power function's change form.

**Keywords** Basalt fiber · Saturated sand · Cyclic triaxial test · Excess pore water pressure (EPWP) · Liquefaction resistance · Dynamic strength curves

## Introduction

As an effective soil improvement technology, reinforcement technology has been widely used in slope protection [1, 2], roadbed treatment [3–5], retaining walls [6–8], and other projects [9, 10]. The traditional reinforcement technology is to arrange the reinforcement material of the soil in a certain direction. The directional distribution will form a potential fracture surface in the soil and increase the soil's anisotropy [11, 12]. The fiber reinforcement technology's objective is to randomly distribute discrete fiber materials in the soil to achieve improvement of the soil's mechanical properties [13, 14]; the randomly distributed fiber materials can well solve the problem of soil anisotropy caused by traditional reinforcement technology [15–20]. As a result, the fiber reinforcement technology is finding wider application in the field of geotechnical engineering, also becoming one of researchers' major concerns.

Fiber-reinforced soil is a common roadbed treatment method, and its dynamic characteristics, especially its liquefaction characteristics under dynamic load, is an important research topic. Eyyüb [21] analyzed the liquefaction resistance of sand with different fiber content and different fiber length and found that the cycle number for

---

✉ Yu Jia  
jia\_yu@csu.edu.cn

Yu Ding  
ding\_yu0212@163.com

Xuan Wang  
dddebug@csu.edu.cn

Jiasheng Zhang  
zjsdj@csu.edu.cn

Xiaobin Chen  
chen\_xiaobin@csu.edu.cn

<sup>1</sup> School of Civil and Ocean Engineering, Jiangsu Ocean University, Lianyungang 222002, Jiangsu, China

<sup>2</sup> Department of Civil Engineering, Central South University, Changsha 410083, Hunan, China



(a)



(b)

Fig. 1 Test materials: a The ISO sand, b Basalt fiber

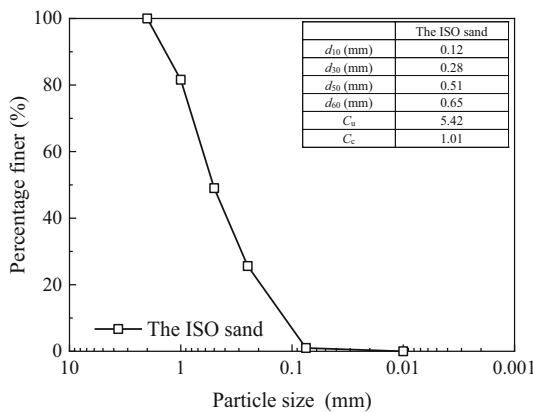


Fig. 2 PSD curve of the ISO sand

Table 1 Physical and mechanical parameters of the ISO sand

Test material	$\rho_{d,max}/(g\ cm^{-3})$	$\rho_{d,min}/(g\ cm^{-3})$	$G_s$	$e$
The ISO sand	1.90	1.64	2.65	0.47

The void ratio  $e$  in the table is corresponding to 95% compaction

Table 2 Basic technical index of basalt fiber

Test material	Density $\rho/(g\ cm^{-3})$	Monofilament diameter $\mu m$	Tensile strength/MPa	Elastic modulus $E/GPa$	Elongation at break $\%$
Basalt fiber	2.63 ~ 2.65	7 ~ 15	3000 ~ 4800	91 ~ 110	3.2

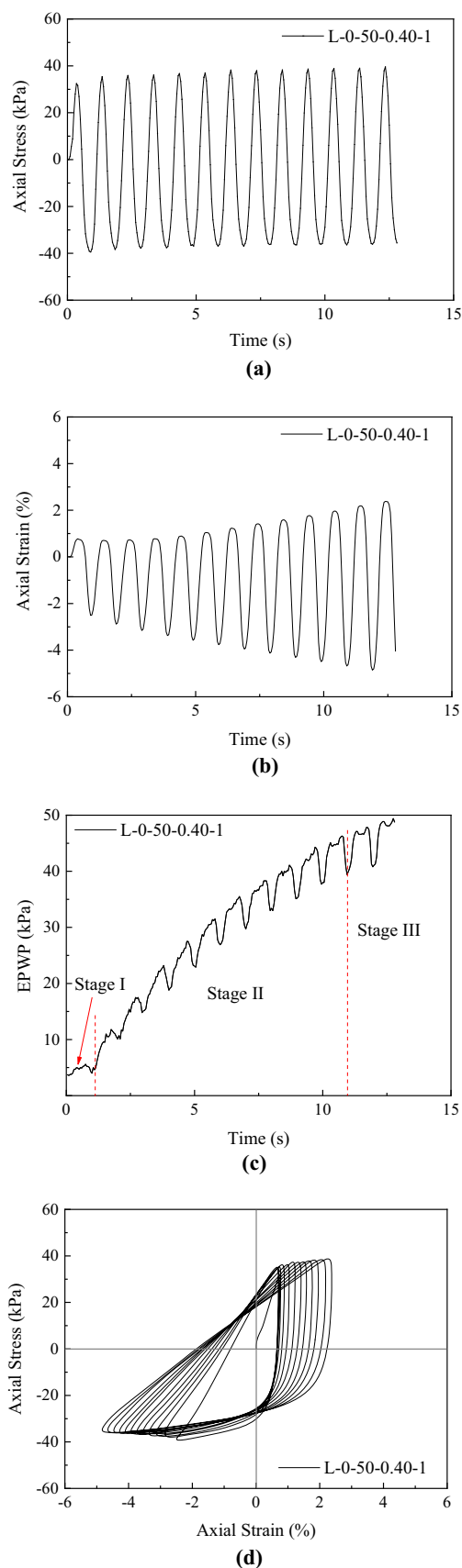
The data in the table are provided by the basalt fiber manufacturer

Table 3 Dynamic triaxial testing programs

No	FC/%	CSR	$f/Hz$	Confining pressure/kPa	Compactness $\%$
1	0	0.30	1	50	95
2	0	0.30	3	50	95
3	0	0.30	5	50	95
4	0	0.35	1	50	95
5	0	0.40	1	50	95
6	0.2	0.30	1	50	95
7	0.2	0.30	3	50	95
8	0.2	0.30	5	50	95
9	0.2	0.35	1	50	95
10	0.2	0.40	1	50	95
11	0.4	0.30	1	50	95
12	0.4	0.35	1	50	95
13	0.4	0.40	1	50	95

Numbers are used to represent each group of tests in the following text, and the numbered rule is: L-FC- $\sigma_3$ -CSR- $f$ . For example, L-0.2%-50-0.30-1 refers to the test with fiber content of 0.2%, confining pressure of 50 kPa, cyclic stress ratio of 0.30, and loading frequency of 1 Hz.

liquefaction increased with the increase in fiber content and fiber length. Zhou [22] studied the liquefaction resistance of calcareous sands reinforced with polypropylene fibers, and the results indicated that increasing fiber content and fiber length could improve the liquefaction resistance of calcareous sands, especially when the fiber content was greater than 0.8%. Fardad [23] studied the liquefaction characteristics of Babolsar sand reinforced with randomly distributed fibers using an energy-based approach, and the results revealed that the addition of fibers increased the number of cycles required to liquefaction, resulting in higher cumulative dissipated energy. Maheshwari [24] conducted shaking table tests on saturated sand with three different reinforced materials (geogrid-plate, geosynthetic fiber, and natural coconut shell fiber) and found that the addition of the three reinforced materials would reduce the maximum pore water pressure ratio, especially with a higher fiber (or geogrid-plates) content. Vercueil [25] implemented cyclic triaxial tests on geosynthetics-



**Fig. 3** Typical test curves for saturated sand: **a** time history curve for axial stress, **b** time history curve for axial strain, **c** time history curve for EPWP, and **d** hysteresis curve

reinforced sand and concluded that geosynthetics can significantly improve the sand's liquefaction resistance. Li [26] discussed the effects of fiber content and fiber length on the excess pore water pressure and dynamic strength. The results showed that with the increasing of fiber content, the dynamic strength and liquefaction resistance increased, whereas the accumulation rate of excess pore water pressure decreased. Zhou [27] conducted a series of cyclic triaxial tests on sisal fiber reinforced sand and concluded that the fiber content has a significant effect on the excess pore water pressure in saturated sand, and the accumulation rate of excess pore water pressure was negatively related with the fiber content. In addition, the interlocking structure formed between fibers and sand particles can significantly improve the liquefaction resistance of sand. However, Wang [28] studied the liquefaction and settlement characteristics of fiber-reinforced saturated sand through centrifugal test and believed that the fiber had no significant influence on the excess pore water pressure and settlement.

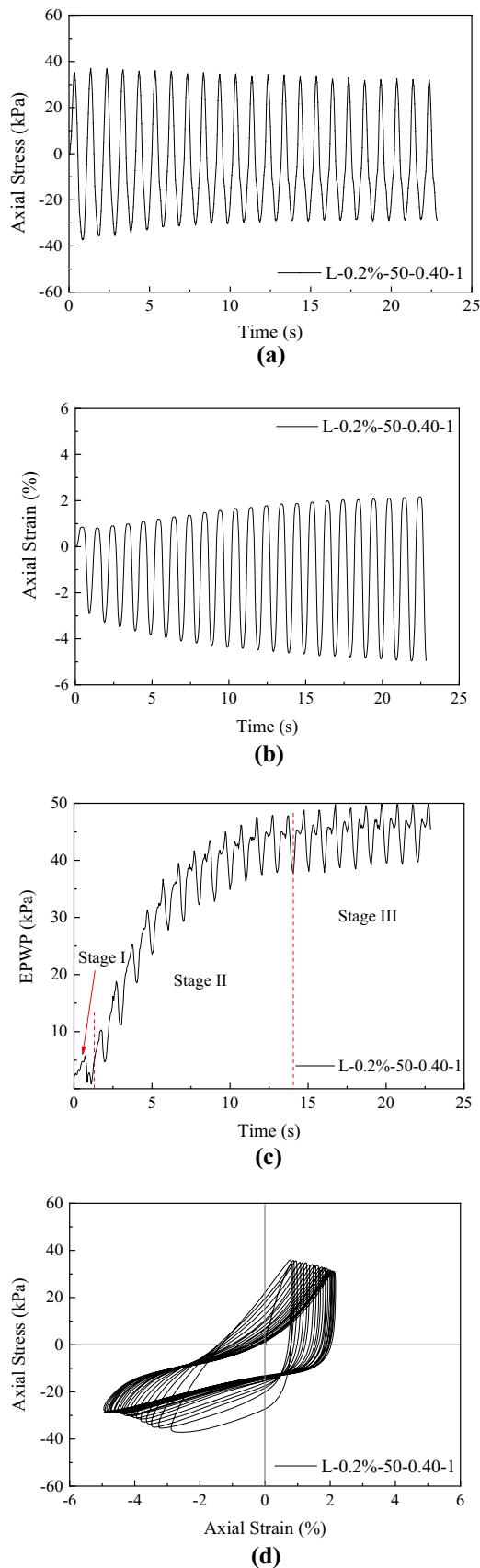
Presently, only a few studies have focused on the liquefaction characteristics of fiber-reinforced saturated sand [29], and the conclusions drawn by existing studies are not consistent. Therefore, it is necessary to implement further research on the liquefaction characteristics of fiber-reinforced saturated sand. In this paper, the influences of fiber content (FC), cyclic stress ratio (CSR), and loading frequency ( $f$ ) on the excess pore water pressure (EPWP) characteristics and the liquefaction characteristics of saturated sand and fiber-reinforced saturated sand were studied through cyclic triaxial test.

## Test Materials and Testing Methods

### Test Materials

The China ISO standard sand was selected as the test material, as shown in Fig. 1a, and the shape of the particles is sub-round to round. Figure 2 shows the particle size distribution (PSD) curve for the ISO sand, and Table 1 lists the physical and mechanical parameters such as the specific gravity and the maximum and minimum unit weights [30].

The fiber used in the test is basalt fiber, which is a fibrous material extracted from natural basalt and has the advantages of high strength, corrosion resistance, and high temperature resistance [31, 32]. In recent years, the mechanical properties of basalt fiber-reinforced soil have become a new research hotspot.



◀**Fig. 4** Typical test curves for basalt fiber-reinforced saturated sand (FC = 0.2%): **a** time history curve for axial stress, **b** time history curve for axial strain, **c** time history curve for EPWP, and **d** hysteresis curve

The length of the basalt fiber selected in this paper is 12 mm, as shown in Fig. 1b, and its basic technical index such as the density, the monofilament diameter, the tensile strength, the elastic modulus, and the elongation at break are all shown in Table 2.

**Testing Methods**

*Testing Equipment*

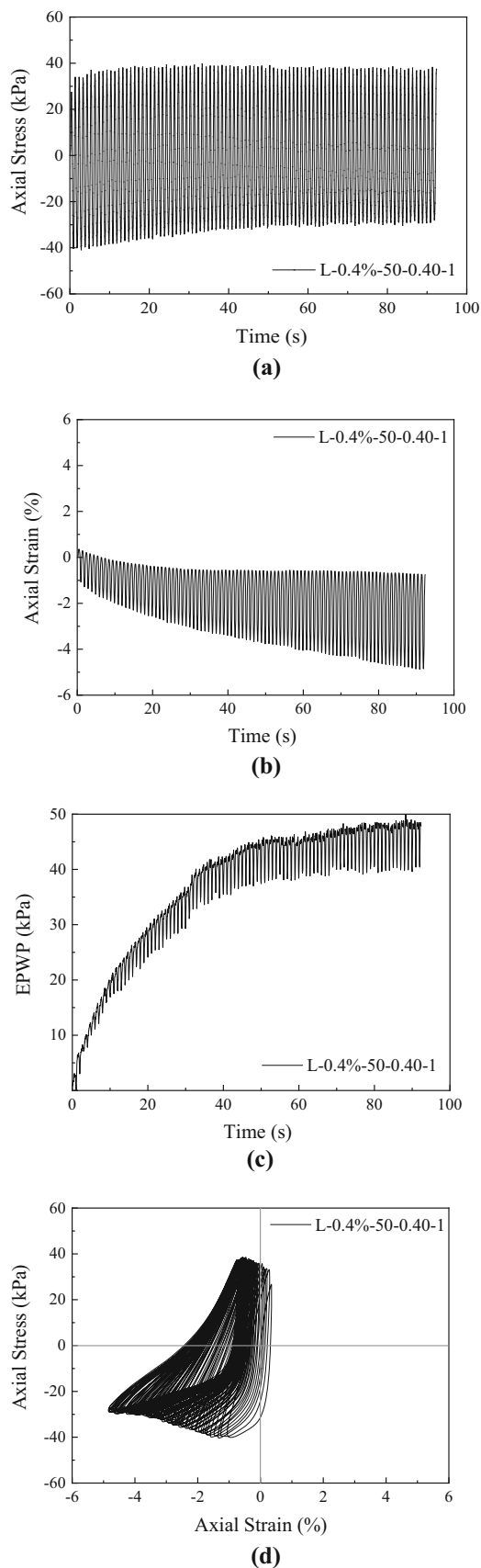
The consolidated undrained cyclic triaxial test was performed with DDS-70 to explore the liquefaction characteristics of basalt fiber-reinforced saturated sand. The equipment is mainly composed of a confining pressure control room, three-axis chamber, vibration exciter, electrical control system, and the equipment can be used for sand liquefaction test.

*Testing Programs*

This paper mainly analyzes the influence of basalt fiber content (i.e., the ratio of the basalt fiber’s weight to the dry sand’s weight, expressed as FC = 0, 0.2%, 0.4%; after 0.4%. This fiber content is reasonable for fibre-reinforcement because fiber contents less than 1% were usually used in previous investigations[24, 28, 33], In addition, we found in our preliminary tests that when the fiber content was above 0.4%, the mixing of soil-fiber was felt very difficult as the fibers are sticking together to form lumps.), the cyclic stress ratio (that is, the ratio of half of the dynamic load amplitude to the confining pressure, expressed with CSR,  $CSR = 0.30, 0.35, 0.40$ ), and the loading frequency ( $f = 1, 3, 5$  Hz) on the excess pore water pressure (EPWP) and the dynamic strength curve of basalt fiber-reinforced saturated sand. The confining pressure is 50 kPa, and the loading waveform is sinusoidal. The test is stopped when the strain reaches 5% or the EPWP equals confining pressure. The specific test programs are shown in Table 3.

*Specimen Preparation*

The diameter of the specimen was 39.1 mm and the height was 80 mm. The specimen was prepared by the layered moist compaction method. The weight of the sand and the basalt fiber required to prepare a specimen was calculated according to the materials’ dry density and fiber content,



◀**Fig. 5** Typical test curves for basalt fiber-reinforced saturated sand (FC = 0.4%): **a** time history curve for axial stress, **b** time history curve for axial strain, **c** time history curve for EPWP, and **d** hysteresis curve

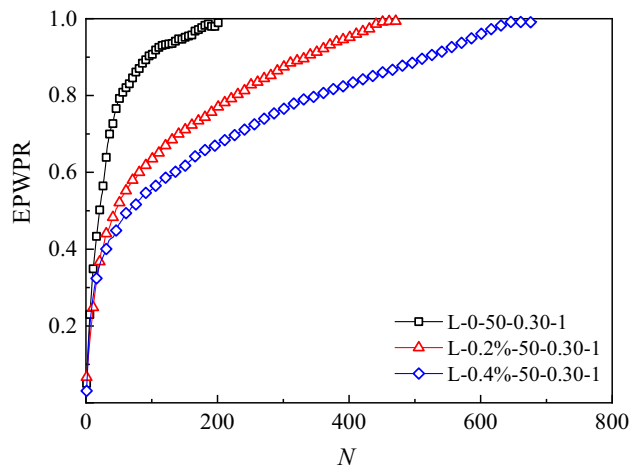


**Fig. 6** The influence of basalt fiber content on the curves of EPWPR and  $N$

etc. Then the sand and the fiber were evenly mixed; a certain amount of distilled water was sprayed to ensure that the mixture had a certain pseudo-cohesion to facilitate specimen preparation. Afterward, the moist mixture was placed in a sealed glassware for 24 h to allow the moisture to be evenly distributed. The specimen was compacted with five layers with a height of 16 mm in each layer. Before pouring into the next layer, the top of previous layer had to be scarified prior to ensure good contact between the two different layers. After the specimen was prepared, it was installed in the triaxial cell for saturation. When the pore pressure coefficient ( $B$ ) was greater than 0.95, the specimen was considered to be saturated. Then, isotropic consolidation was carried out under a predetermined confining pressure. Finally, dynamic load was applied to perform the test.

## Test Results

### Analysis of Typical Test Curves

Figures 3, 4, and 5 show typical test curves for saturated sand and basalt fiber-reinforced saturated sand obtained from cyclic triaxial test, where (a) is the time history curve for axial stress, (b) is the time history curve for axial strain, (c) is the time history curve for EPWP, and (d) is the hysteresis curve. It can be seen from Figs. 3, 4, 5 that: (1)

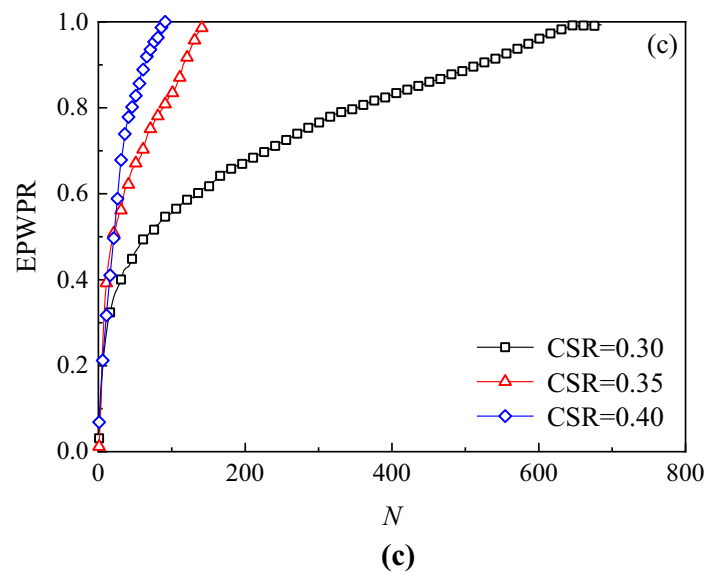
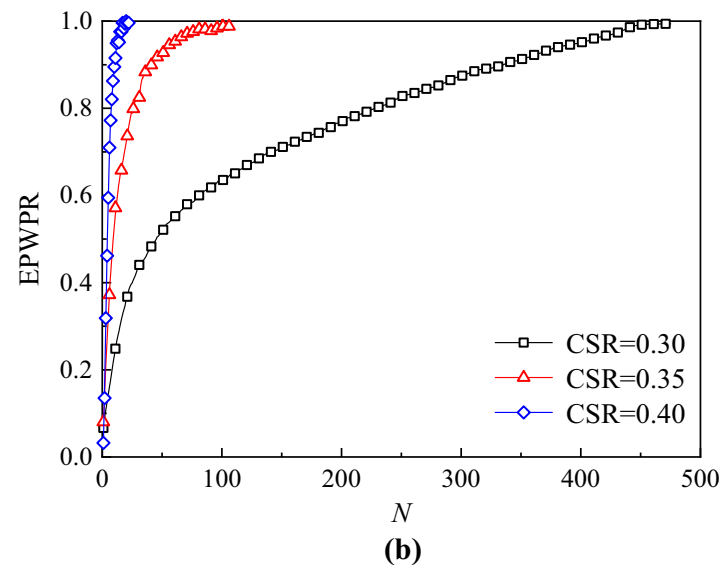
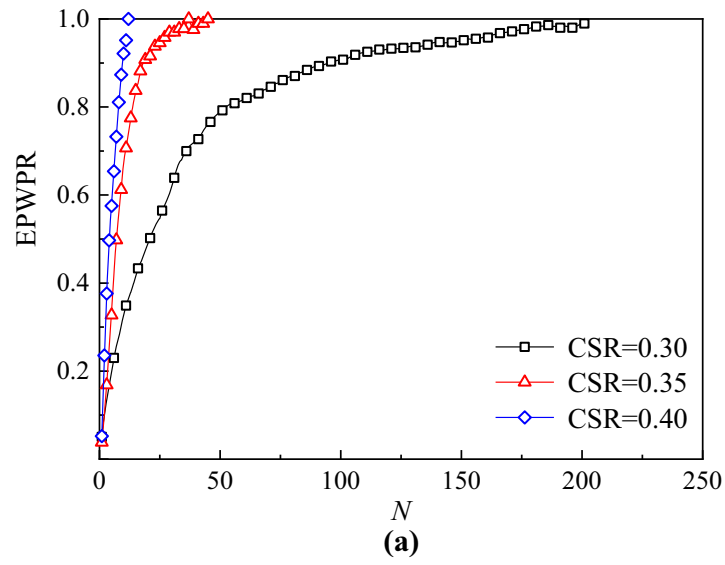


**Fig. 7** The influence of CSR on the curves of EPWPR and  $N$ : **a** Saturated sand, **b** Basalt fiber-reinforced saturated sand with FC = 0.2%, **c** Basalt fiber-reinforced saturated sand with FC = 0.4%

the axial stress shows a sinusoidal wave trend, and as the loading progresses, the axial stress slightly decreases. (2) The axial strain presents a horn shape, and as the loading progresses, the axial strain increases in the form of sine wave until the axial strain reaches 5%. (3) The curves of EPWP and loading time can be divided into three stages. At the initial stage of loading (stage I), the EPWP presents irregular changes. In the middle stage of loading (stage II), the EPWP increases rapidly in a sinusoidal wave. At the later stage of loading (stage III), the sample achieves initial liquefaction and the EPWP increases slowly in the form of sine wave, and at this stage, there is a groove at each peak of sine wave. (4) As the time go on, the long axis of the hysteretic curve gradually shifts horizontally and the

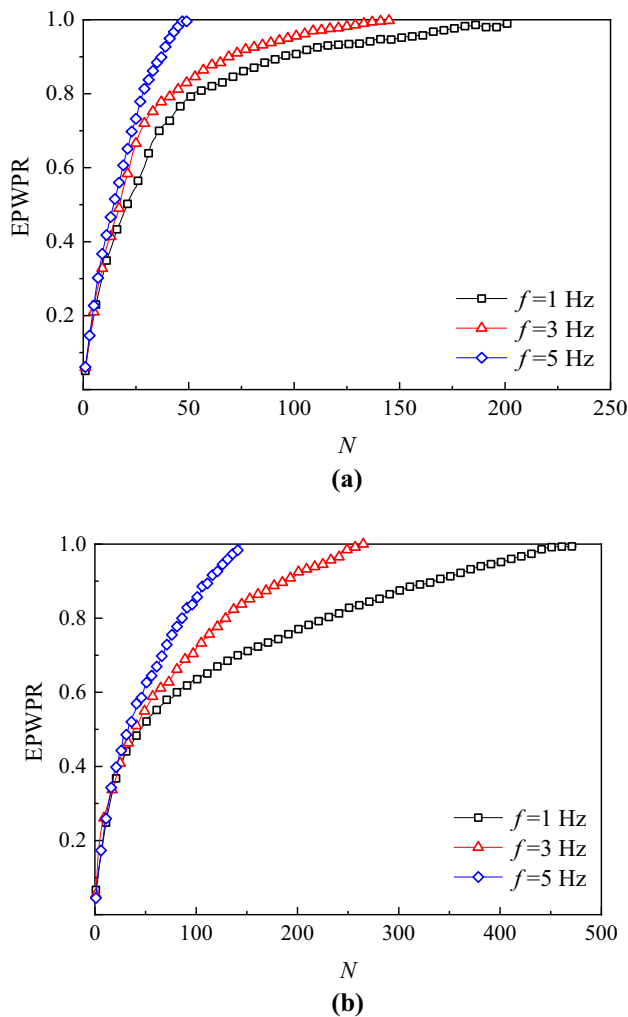


**Fig. 8** The influence of loading frequency on curves of EPWPR and cycle number: **a** Saturated sand, **b** Basalt fiber-reinforced saturated sand with FC = 0.2%

**Table 4** Fitting parameters for Eq. (1)

Test no.	$a$	$b$	$R^2$
L0-50-0.30-1	0.905	0.010	0.996
L0-50-0.351	0.779	0.172	0.937
L0-50-0.40-1	0.418	0.562	0.989
L0-50-0.30-3	0.874	0.115	0.994
L0-50-0.30-4	0.581	0.392	0.998
L0.2%-50-0.30-1	0.938	0.123	0.935
L0.2%-50-0.35-1	0.898	0.087	0.994
L0.2%-50-0.40-1	0.706	0.228	0.909
L0.2%-50-0.30-3	0.858	0.178	0.979
L0.2%-50-0.30-5	0.742	0.289	0.992
L0.4%-50-0.30-1	0.957	0.124	0.916
L0.4%-50-0.35-1	0.913	0.179	0.923
L0.4%-50-0.40-1	0.715	0.273	0.996

hysteresis curve becomes flat, which indicates that the specimen’s stiffness and elastic modulus are gradually reduced with loading. The hysteresis curve’s area also gradually increases with an increase in loading time, which indicates that the energy consumed by the specimen gradually increases; that is, the damping ratio of the specimen gradually increases.

**Analysis on Characteristics of Excess Pore Water Pressure Ratio**

*The Influence of Basalt Fiber Content on Excess Pore water pressure ratio*

In the following analysis, the EPWP was normalized by the confining pressure and obtain the excess pore water pressure ratio (EPWPR). Figure 6 shows the influence of basalt fiber content on the curves of EPWPR with the cycle number  $N$ . Figure 6 shows that: (1) the EPWPR of saturated sand and basalt fiber-reinforced saturated sand varies with the cycle number, which can be divided into two stages: the EPWPR linearly increases with the cycle number less than 50; when the cycle number is more than 50, the EPWPR nonlinearly increases until it reaches 1.0. Simultaneously, liquefaction failure occurs to the specimen. (2) The EPWPR for a given cycle number decreases with an increase in basalt fiber content, and the cycle number for liquefaction also shows an increasing with the increase of basalt fiber content. For saturated sand, the cycle number for liquefaction is 204; when the basalt fiber content is 0.2%, the cycle number for liquefaction is 475, which is 132.8% higher than that of saturated sand, and when the basalt fiber content is 0.4%, the cycle number for

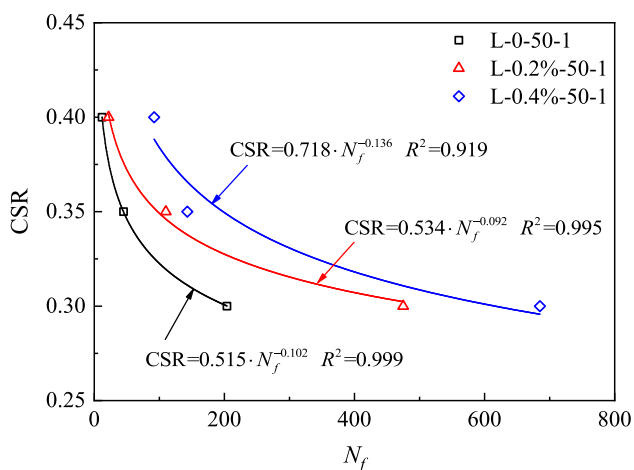


**Fig. 9** Dynamic strength curves for saturated sand and basalt fiber-reinforced saturated sand

liquefaction is 685, which is 235.8% higher than that of saturated sand. This indicates that the addition of basalt fiber can inhibit the generation and accumulation of EPWP in saturated sand, especially with a fiber content of 0.4% (in this paper, the fiber content is limited to 0.4%). This is consistent with the research conclusions of Maheshwari [24], Noorzad [33], and Boominathan [34].

*The Influence of CSRs on EPWPR*

The influence of CSRs on the curves of EPWPR and cycle number are shown in Fig. 7. We can see that the EPWPR of both saturated sand and basalt fiber-reinforced saturated sand increases with an increase in CSR under at a given cycle number, and the cycle number for liquefaction also decreases with the increase of CSR. With an increase of CSR, the stress exerted on the saturated specimen also increases, thus the internal structure of the specimen is more prone to failure, and more excess pore water pressure is accumulated in the saturated specimen.

*The Influence of Loading Frequency on EPWPR*

Figure 8 shows the influence of loading frequency on the curves of EPWPR with cycle number for saturated sand and basalt fiber-reinforced saturated sand (FC = 0.2%). As can be seen from Fig. 8 that for saturated sand and basalt fiber-reinforced saturated sand, the increase of loading frequency is conducive to the accumulation of EPWP and accelerates the process of soil liquefaction failure. When the loading frequency is higher, the time of one stress cycle applied to the saturated specimen is shorter, and the EPWP generated inside the specimen has not enough time to dissipate before the next cyclic loading begins. And it is

easier to accumulate excess pore water pressure, thus the specimen is more prone to liquefaction failure.

**Empirical Model of EPWPR**

To eliminate the influence of cycle number, it is normalized by the cycle number for liquefaction (i.e., cycle number ratio,  $N/N_f$ ). The curves of the EPWPR and the cycle number ratio satisfy the hyperbolic form. According to Chen [35], the curves of the EPWPR and the cycle number ratio can be fitted by hyperbolic function, as shown in Eq. (1).

$$\frac{u_d}{\sigma_3} = \frac{N/N_f}{a(N/N_f) + b} \tag{1}$$

where  $u_d$  is the EPWP,  $\sigma_3$  is the confining pressure,  $N$  is the cycle number,  $N_f$  is the cycle number for liquefaction,  $a$  and  $b$  are the fitting parameters that determine the influence of cycle number. Equation (1) is used to fit the curves of EPWPR and cycle number ratio, and the fitting parameters  $a$  and  $b$ , and the correlation coefficients  $R^2$  are obtained as shown in Table 4; we know that the  $R^2$  are all greater than 0.90, which indicates that the empirical model can well predict the development of EPWP for saturated sand and basalt fiber-reinforced saturated sand well.

**Dynamic Strength Curve**

The cyclic number for liquefaction and the corresponding cyclic stress ratio were plotted in a graph, and we obtain the dynamic strength curves for saturated sand and basalt fiber-reinforced saturated sand with different fiber content as shown in Fig. 9. It can be seen that for both saturated sand and basalt fiber-reinforced saturated sand, the cycle number for liquefaction decreases with the increase of CSR. For a given cycle number, larger cyclic stress ratio was required for specimen to liquefaction as the fiber content increased. This also verifies that an addition in fibers greatly improve the liquefaction resistance of saturated sand. In this paper, when the fiber content is 0.4%, the liquefaction resistance of fiber-reinforced sand is the most optimal. Additionally, the curves of CSR and the cycle number for liquefaction are in the form of a power function, according to Zhou [36], it can be calculated by a power function, as shown in Eq. (2).

$$CSR = m \cdot N_f^n \tag{2}$$

where  $m$  and  $n$  are fitting parameters, Eq. (2) is used to fit the dynamic strength curves for saturated sand and basalt fiber-reinforced saturated sand. The obtained fitting parameters and the correlation coefficients  $R^2$  are shown in Fig. 9. The correlation coefficients are all greater than 0.90, indicating that Eq. (2) can well describe the dynamic



strength curves for saturated sand and basalt fiber-reinforced saturated sand.

## Conclusion

This paper studies the liquefaction characteristics of saturated sand and basalt fiber-reinforced saturated sand by cyclic triaxial test and draws the following conclusions:

1. An addition in basalt fiber can effectively inhibit the generation and accumulation of EPWP and improve the liquefaction resistance of saturated sand; the liquefaction resistance of fiber-reinforced saturated sand increases with the increase of basalt fiber content, and the optimal basalt fiber content is about 0.4%.
2. For saturated sand and basalt fiber-reinforced saturated sand, the increase in CSR and the increase in loading frequency are beneficial to the accumulation of EPWPR and accelerate the process of soil liquefaction failure.
3. The curves of EPWP and loading time can be divided into three stages: stage I, the EPWP presents irregular changes; stage II, the EPWP increases rapidly in a sinusoidal wave; and stage III, the EPWP increases slowly in the form of sine wave. The curves of EPWPR and cycle number ratio for saturated sand and basalt fiber-reinforced saturated sand is in accordance with the hyperbolic function, and an empirical model to predict EPWP was proposed.
4. The cycle number for liquefaction decreases with the increase of CSR. The dynamic strength curves for saturated sand and basalt fiber-reinforced saturated sand conform to the power function.

**Acknowledgements** The author is grateful to the anonymous reviewers for their constructive comments and suggestions. The authors also thank AiMi Academic Services ([www.aimieditor.com](http://www.aimieditor.com)) for their English language editing and review services.

**Funding** The study was supported by the National Natural Science Foundation of China (51978674).

## Declarations

**Conflict of interest** The authors declare that they have no conflict of interest.

## References

1. Zhang R, Long MX, Lan T, Zheng JL, Geoff C (2020) Stability analysis method of geogrid reinforced expansive soil slopes and its engineering application. *J Central South Univ* 27(7):1965–1980. <https://doi.org/10.1007/s11771-020-4423-x>
2. Zheng BB, Zhang DM, Liu WS, Yang YH, Yang H (2019) Use of basalt fiber-reinforced tailings for improving the stability of tailings dam. *Materials* 12(8):1306–1315. <https://doi.org/10.3390/ma12081306>
3. Ramesh A, Rao CN, Kumar M (2019) Experimental study on geocell and of fibre reinforced soil sub-grade under static and repetitive load. In: Singapore, Singapore, pp 139–149
4. Tan TT, Huat BBK, Anggraini V, Shukla SK, Nahazanan H (2019) Strength behavior of fly ash-stabilized soil reinforced with coir fibers in alkaline environment. *J Nat Fibers*. <https://doi.org/10.1080/15440478.2019.1691701>
5. Saride S, Baadiga R (2021) New layer coefficients for geogrid-reinforced pavement bases. *Indian Geotech J* 51(1):182–196. <https://doi.org/10.1007/s40098-020-00484-6>
6. Celik S, Ghalehjouhl BK, Majedil P, Akbulut S (2017) Effect of randomly fiber reinforcement on shear failure surface of soil, behind flexible retaining walls at different conditions. *Indian J Geo-Marine Sci* 46(10):2097–2104
7. Grishina AS, Ponomaryov AB (2016) Analysis of efficiency of fiber reinforced sand as a backfill of retaining walls. Proceedings of the 8th Asian Young Geotechnical Engineers Conference, August 5–7, Astana, Kazakhstan
8. Ling HI, Xu L, Leshchinsky D, Collin G, Rimoldi P (2016) Centrifugal modeling of reinforced soil retaining walls considering staged construction. *Geo-Chicago*, August 14–18, Chicago, United states
9. Krishna AM, Biswas A (2021) Performance of geosynthetic reinforced shallow foundations. *Indian Geotech J* 51(3):583–597. <https://doi.org/10.1007/s40098-021-00546-3>
10. Dash SK, Shivadas AS (2012) Performance improvement of railway ballast using geocells. *Indian Geotech J* 42(3):186–193. <https://doi.org/10.1007/s40098-012-0017-3>
11. Estabragh AR, Bordbar AT, Javadi AA (2011) Mechanical behavior of a clay soil reinforced with nylon fibers. *Geotech Geol Eng* 29(5):899–908. <https://doi.org/10.1007/s10706-011-9427-8>
12. Wang YX, Guo PP, Ren WX, Yuan BX, Yuan HP, Zhao YL, Shan SB, Cao P (2017) Laboratory investigation on strength characteristics of expansive soil treated with jute fiber reinforcement. *Int J Geomech* 17(11):04017101. [https://doi.org/10.1061/\(ASCE\)GM.1943-5622.0000998](https://doi.org/10.1061/(ASCE)GM.1943-5622.0000998)
13. Rong DZ, Tang CS, Zeng H, Cheng Q, Li HD, Shi B (2021) Evaporation process and tensile behavior of fiber reinforced rammed earth. *Chin J Geotech Eng* 43(04):670–678. <https://doi.org/10.11779/CJGE202104009>
14. An N, Yan CG, Wang YC, Lan HX, Bao H, Xu JB, Shi YL, Sun WF (2021) Experimental study on anti-erosion performance of polypropylene fiber-reinforced loess. *Rock Soil Mech* 42(02):501–510. <https://doi.org/10.16285/j.rsm.2020.0879>
15. Xu J, Wu ZP, Che H, Shao LT, Zhou XG, Wang SH (2021) Triaxial shear behavior of basalt fiber-reinforced loess based on digital image technology. *KSCE J Civ Eng* 25:3714–3726. <https://doi.org/10.1007/s12205-021-2034-1>
16. Huang XL, Ding Y, Xu WN, Xiong SY, Liu LM (2021) Mechanical performance of vegetation-growing concrete reinforced by palm fibers under triaxial compression. *KSCE J Civ Eng* 25:4610–4619. <https://doi.org/10.1007/s12205-021-2160-9>
17. Li G, Zhang JL, Liu J (2019) Experimental study on the shear behaviors of polypropylene fiber-reinforced sand. *KSCE J Civ Eng* 23:4992–5001. <https://doi.org/10.1007/s12205-019-0794-7>
18. Liu J, Wang GH, Kamai T, Zhang FY, Yang J, Shi B (2011) Static liquefaction behavior of saturated fiber-reinforced sand in undrained ring-shear tests. *Geotext Geomembr* 29(5):462–471. <https://doi.org/10.1016/j.geotextmem.2011.03.002>
19. Tang CS, Shi B, Gao W, Chen FY, Cai Y (2007) Strength and mechanical behavior of short polypropylene fiber reinforced and

- cement stabilized clayey soil. *Geotext Geomembr* 25(3):194–202. <https://doi.org/10.1016/j.geotextmem.2006.11.002>
20. Prabakar J, Sridhar RS (2002) Effect of random inclusion of sisal fibre on strength behaviour of soil. *Constr Build Mater* 16(2):123–131. [https://doi.org/10.1016/S0950-0618\(02\)00008-9](https://doi.org/10.1016/S0950-0618(02)00008-9)
  21. Eyyüb K, Tuğba E, Selim A (2018) The liquefaction behavior of poorly graded sands reinforced with fibers. *Adv Civ Eng*. <https://doi.org/10.1155/2018/4738628>
  22. Zhou L, Chen JF, Peng M, Zhu Y (2022) Liquefaction behavior of fiber-reinforced calcareous sands in unidirectional and multi-directional simple shear tests. *Geotext Geomembr* 50:794–806. <https://doi.org/10.1016/j.geotextmem>
  23. Fardad AP, Noorzad R (2017) Energy-based evaluation of liquefaction of fiber-reinforced sand using cyclic triaxial testing. *Soil Dyn Earthq Eng* 104:45–53. <https://doi.org/10.1016/j.soildyn.2017.09.026>
  24. Maheshwari BK, Singh HP, Saran S (2012) Effects of reinforcement on liquefaction resistance of Solani sand. *J Geotech Geoenviron Eng* 138(7):831–840. [https://doi.org/10.1061/\(asce\)gt.1943-5606.0000645](https://doi.org/10.1061/(asce)gt.1943-5606.0000645)
  25. Vercueil D, Billet P, Cordary D (1997) Study of the liquefaction resistance of a saturated sand reinforced with geosynthetics. *Soil Dyn Earthq Eng* 16(7):417–425. [https://doi.org/10.1016/S0267-7261\(97\)00018-3](https://doi.org/10.1016/S0267-7261(97)00018-3)
  26. Li G, Zhang JL, Liu J (2020) Mechanical response of fiber-reinforced sand under cyclic loading. *E3S Web of Conf* 198:01048. <https://doi.org/10.1051/e3sconf/202019801048>
  27. Zhou LL, Su L, Ling XZ, Liu X, Guan D, Zhang YQ (2021) Experimental and numerical modeling on liquefaction resistance of fiber reinforced sand. *J Eng Geol* 29(05):1567–1576. <https://doi.org/10.13544/j.cnki.jeg.2021-0381>
  28. Wang K, Brennan A (2019) Behaviour of saturated fibre-reinforced sand in centrifuge model tests. *Soil Dyn Earthq Eng* 125:38–48. <https://doi.org/10.1016/j.soildyn.2019.105749>
  29. Liu C, Bin YE, Lu JF (2014) Research progress on the liquefaction resistance of characteristics of fiber-reinforced soil. *Chin J Geol Hazard Control* 25(04):108–113. <https://doi.org/10.16031/j.cnki.issn.1003-8035.2014.04.021>
  30. TB10102-2010 Code for soil test of railway engineering (2010) China Railway Publishing House, Beijing, China
  31. Lai TW, Lei H, Wu ZX, Wu HG (2021) Shaking table test study on basalt fiber reinforced plastics in high slope protection. *Rock Soil Mech* 42(02):390–400. <https://doi.org/10.16285/j.rsm.2020.0851>
  32. Xue WP, Gao C, Shen L, Liu XY (2020) Effect of confining pressure on permeability and pore structure of basalt fiber reinforced concrete after high temperature. *J Build Mater*. <https://doi.org/10.3969/j.issn.1007-9629.2021.04.010>
  33. Noorzad R, Amini PF (2014) Liquefaction resistance of Babolsar sand reinforced with randomly distributed fibers under cyclic loading. *Soil Dyn Earthq Eng* 66:281–292. <https://doi.org/10.1016/j.soildyn.2014.07.011>
  34. Boominathan A, Hari S (2002) Liquefaction strength of fly ash reinforced with randomly distributed fibers. *Soil Dyn Earthq Eng* 22(9–12):1027–1033. [https://doi.org/10.1016/S0267-7261\(02\)00127-6](https://doi.org/10.1016/S0267-7261(02)00127-6)
  35. Chen GX, Liu XZ (2004) Study on dynamic pore water pressure in silty clay interbedded with fine sand of Nanjing. *Chin J Geotech Eng* 26(1):79–82. <https://doi.org/10.3321/j.issn:1000-4548.2004.01.015>
  36. Zhou EQ, Wang Q, Zong ZX, Lu JF (2019) Cyclic triaxial tests on dynamic characteristics of saturated rubber-sand mixture. *Rock Soil Mech* 40(10):3797–3804. <https://doi.org/10.16285/j.rsm.2018.1552>

**Publisher's Note** Springer Nature remains neutral with regard to jurisdictional claims in published maps and institutional affiliations.

Springer Nature or its licensor (e.g. a society or other partner) holds exclusive rights to this article under a publishing agreement with the author(s) or other rightsholder(s); author self-archiving of the accepted manuscript version of this article is solely governed by the terms of such publishing agreement and applicable law.